Analytica Chimica Acta 1365 (2025) 344246

Contents lists available at ScienceDirect

Analytica Chimica Acta

journal homepage: www.elsevier.com/locate/aca

A direct, real-time, size-resolved analytical strategy to follow drug loading and release from biocompatible gold nanoparticles

Valentina Marassi [a,b,c,1], Junjie Wang [a,1], Stefano Giordani [a,b,c], Anna Placci [a,b,c], Barbara Roda [a,b,c], Pierluigi Reschiglian [a,b,c], Andrea Zattoni [a,b,c,*]

[a] Department of Chemistry G. Ciamician, University of Bologna, 40126, Bologna, Italy
[b] byFlow srl, 40129, Bologna, Italy
[c] INBB – Biostructures and Biosystems National Institute, 00136, Rome, Italy

HIGHLIGHTS

- Multi-technique (UV, DLS, AF4) analysis optimized Au-BSA-CUR drug carrier synthesis and loading efficiency.
- AF4-DAD used A_{401}/A_{530} ratio to monitor real-time drug release with full-load value of 0.77 ± 0.01.
- AF4 enabled first-time monitoring of drug aggregation at low temperatures during release.
- AF4-DAD-MALS reliably studies nanoparticle drug system stability, loading, and release behavior.

GRAPHICAL ABSTRACT

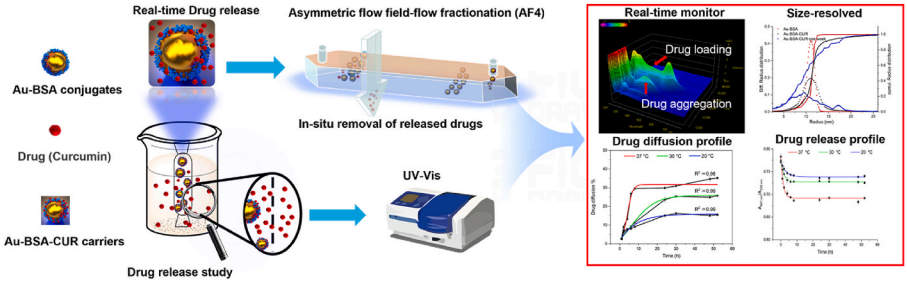

ARTICLE INFO

Keywords:
Asymmetric flow field-flow fractionation (AF4, FFF)
Gold nanoparticle (AuNPs)
Albumin-nanoparticle conjugates
Curcumin drug delivery
Real-Time Drug Release Monitoring
Multi-Detector Characterization (MALS, DAD, UV–Vis)
Simulated Physiological Conditions

ABSTRACT

Background: Analytical methods for the characterization of nanoparticle-based drug delivery systems often rely on the quantification of unbound drug to provide information on drug loading and delivery, but fail to account for system complexity, address the state of the releasing system, or simulate the physiological environment. There is a clear need for new analytical methods capable of following the entire process of drug loading, stability and release under physiological conditions, based on multi-parametric analytical platforms. Asymmetric flow field-flow fractionation (AF4) can be used to size sort and isolate nanoparticles for further analysis or characterization by online, uncorrelated techniques.

Results: We propose AF4 coupled with online multiple detectors to investigate the model drug delivery system consisting of albumin (BSA)-coated gold nanoparticles (AuNPs) loaded with curcumin (CUR). A maximum loading efficiency of 88.9 % is achieved by optimizing various experimental parameters. The absorbance ratio of nanocarriers at 401 nm and 530 nm was successfully proposed as an index for evaluating drug loading (full load was 0.77 ± 0.01) and release from the carrier surface. At 37 °C, Au-BSA-CUR exhibits rapid drug release, achieving 34.8 % total release. This process is accompanied by swift degradation and efficient diffusion of the drug into the surrounding reservoir (~30 %). The appearance of new absorbance peaks in fractograms (curcumin aggregation) at lower temperatures (20 or 30 °C) indicates the special properties of hydrophobic drugs, which are monitored by the AF4 platform for the first time.

* Corresponding author. Department of Chemistry G. Ciamician, University of Bologna, 40126 Bologna, Italy.
E-mail address: andrea.zattoni@unibo.it (A. Zattoni).
[1] Contributed equally.

https://doi.org/10.1016/j.aca.2025.344246
Received 21 January 2025; Received in revised form 22 May 2025; Accepted 23 May 2025
Available online 24 May 2025

Significance: The tailored strategy employed in our investigation provided detailed, real-time, in situ analysis, making it a powerful tool for designing and optimizing drug delivery systems, providing insight into both loading and release mechanisms, assessing nanoparticle stability, and tolerating saline media. These results suggest that AF4-DAD-MALS is a more reliable and insightful technique for studying the stability, loading efficiency, and release dynamics of nanoparticle-based drug delivery systems.

1. Introduction

Nanosized drug delivery systems have demonstrated their potential to mitigate the shortcomings of traditional drugs in terms of poor bioavailability, specificity, low solubility, cytotoxicity, and insufficient accumulation in the body. In such systems the conventional molecular drug is administered after loading on top or inside the nanosized carrier. In most cases, such systems also involve the use of a coating agent to promote the stability of the device in vivo (e.g. albumin for hemocompatibility) [1]. Of course, the intrinsic complexity of such systems compared to the single molecular drugs requires a more complex characterization, which needs to be increasingly thorough as the nanodevice becomes more complex [2].

Gold nanoparticles (AuNPs), with their diverse geometries, have gained prominence in the field of nanomedicine due to their outstanding optical properties, versatile functionalization capabilities, and precisely controlled drug release mechanisms [3,4]. In addition, the localized surface plasmon resonance (LSPR) property of AuNPs is highly dependent on their size, shape, and the surrounding environment. This tunability makes them highly suitable for precise biosensing and detection applications [5,6]. Therefore, their unique optical properties enable them not only to transport and release therapeutic agents, but also to monitor the target site and perform photothermal therapy, thereby enhancing the overall therapeutic efficacy.

Functionalization of AuNPs and modification of endogenous proteins can significantly improve their biocompatibility, selectivity, and resistance to biodegradation. This approach ensures better integration and performance in biological systems [7–9]. Indeed, over the past decade, biomedical applications using AuNP-albumin nanoplatforms have been extensively studied to address the challenges of drug efficacy and selectivity with the aim of improving therapeutic outcomes [10]. Due to its bioaccumulation, targeting capabilities, biocompatibility, and surface properties, albumin can efficiently transport various therapeutic agents to specific sites in the body, thereby enhancing targeted drug delivery [11,12]. In addition, the unique optical properties of AuNPs allow them to be monitored or imaged using multiple detectors. Controlled drug release can be achieved through various mechanisms, including photothermal effects, pH changes, and competitive reactions, providing versatile and responsive drug delivery options [13,14].

Recent advances have explored a range of noble metal nanoparticle systems conjugated with therapeutic agents for targeted delivery and multimodal therapy. For instance, gold nanorods and nanocages have been engineered to realize highly effective synergistic chemo–photothermal tumor treatment, with release of doxorubicin and other chemotherapeutics [14]. Similarly, albumin-functionalized AuNPs have been used to co-deliver imaging and therapeutic agents for enhanced tumor accumulation and optical tracking [10]. Beyond cancer, silver–gold hybrid nanoparticles have shown promise in antimicrobial therapy due to their synergistic release and targeting capabilities [15]. These systems demonstrate the versatility of noble metals in drug delivery, but also underscore persistent analytical challenges.

However, one of the major barriers to the clinical translation of such nanomedicines remains insufficient drug loading and uncontrolled release, which often result in therapeutic inefficacy, batch variability, and higher production costs. Most clinically evaluated nanocarriers incorporate only a few weight percent of the active compound, necessitating large doses of the carrier and raising concerns about scalability and potential toxicity. These limitations are especially critical when high drug doses are required, as in oncology or chronic disease management. In this context, high drug-loading nanocarriers — particularly those based on biocompatible materials — are of great interest, as they may reduce carrier burden while achieving therapeutic thresholds more efficiently [16]. These systems demonstrate the versatility of noble metals in drug delivery but also underscore persistent analytical challenges.

A 2016 study showed that most U.S. Food and Drug Administration (FDA) approved nanoparticle delivery systems are polymer-based and liposome-based NPs [17], but speculated that due to the variety of available and increasingly understood NP-based delivery systems, future trends may shift toward new types of nanoparticles. In a 2021 update work, the authors describe 35 nanoparticles in clinical trials, 28 of which are lipid-based NPs [18]. Although polymeric and lipid matrices have many advantages, there is an urgent need to explore and advance a variety of other forms of delivery systems, such as metal NPs, and translate them into clinical trials.

While the biomedical promise of noble metal nanoparticles is well established, critical challenges remain in accurately characterizing drug loading, carrier stability, and release dynamics in physiologically relevant conditions [19]. This requires a combination of analytical techniques to fully understand and optimize their potential. By far the most popular size and shape characterization techniques are scanning and transmission electron microscopy (SEM, TEM) [20]. However, the special sample preparation requirements of these two techniques hinder their characterization in their native liquid dispersion state. Light scattering (LS) techniques, especially dynamic LS (DLS), are able to monitor the hydrodynamic size distribution range in the liquid dispersion media. Static and multi-angle LS (MALS) can provide more information about NPs, such as conformation, surface properties, and core-shell structure [21]. However, the accuracy of these techniques is limited by the multimodal size distribution and complexity of NPs, especially in the presence of complex aggregates.

Rotello and colleagues have extensively contributed to this field, particularly through ligand engineering strategies that modulate nanoparticle–biomolecule interactions for targeted delivery and sensing [22]. However, many of these approaches rely on offline, endpoint assays or mass spectrometry imaging, which are limited in resolving dynamic processes like drug desorption, carrier aggregation, or intermediate complexation [23].

Flow field-flow fractionation (F4) as a mature separation method can be used to size sort and isolate NPs for further analysis or size/spectroscopic characterization by online, uncorrelated techniques, including MALS, DLS, absorbance and luminescence spectrophotometry, and inductively coupled plasma mass spectrometry (ICP-MS) [24,25]. In particular, the whole separation procedure is performed in an empty capillary channel through an external field applied perpendicularly to a mobile phase flow with an ideally parabolic flow profile, which provides a non-destructive, native size-based separation technique. Therefore, based on the features and advantages of the instrument, it has been widely used in many fields such as food, medicine, biology, etc. [25–28].

The evaluation and monitoring of in vitro drug release from nanosized formulations is even more challenging due to the difficulties in achieving an efficient and rapid separation of the free drug from the encapsulated drug and assuring sink conditions during the experiment [2,29].

The vast majority of the current approaches can be schematized as a two-step procedure involving the separation of the released drug from

the carrier followed by its offline quantification (mostly by HPLC) [30]. Separation is achieved by techniques such as ultracentrifugation, size exclusion chromatography (SEC), centrifugal ultrafiltration, or dialysis. Ultracentrifugation and SEC can alter nanocarriers due to high centrifugal forces, leading to artificial drug release. In contrast, softer approaches such as centrifugal ultrafiltration and dialysis (the most exploited) may be affected by membrane clogging due to their limited compatibility with the species and the experimental conditions considered. All the presented approaches suffer from another major deficiency: they focus only on the quantification of the unbound drug, without considering the complexity of the system. To overcome this limitation, it is necessary to develop a platform capable of quantifying drug release and simultaneously characterizing the state of the carrier and its environment after release.

In contrast, our AF4 system combined with photodiode array and multiangle light scattering detection (AF4-DAD-MALS) addresses these shortcomings by providing real-time, size-resolved separation and spectral analysis in situ. By coupling structural and compositional characterization, this platform allows for simultaneous quantification of unbound drug, carrier-associated species, and potential degradation products under physiological conditions — a capability that directly overcomes the limitations of traditional ultracentrifugation-UV or dialysis-HPLC approaches [15].

Moreover, unlike other approaches proposed in the literature, our methodology provides information on the state of the nanodevice and its environment in the dialysis bag after release under biocompatible conditions, instead of focusing only on the released components.

As a representative drug for the study, we selected curcumin (CUR), which has been reported to have potent antioxidant, antibacterial, anti-inflammatory, and anticancer effects [31,32]. First, the loading of CUR onto the surface of the Au-BSA conjugates not only greatly improves its solubility in aqueous media, but also reduces the degradation of curcumin in aqueous solution. A maximum loading efficiency (LE) of 88.9 % can be achieved. In addition, the gentle AF4 principle can help reduce sample loss and improve stability by compensating for any negative effects of centrifugation. Moreover, with the support of the AF4-DAD platform, we can further detect the changes of different species in the incubation solution. In particular, the independent binding between the drug and excess BSA provides another basis for the quantification of drug loading. Further coupling with online MALS and offline DLS allowed us to monitor the size change of Au-BSA-Cur carrier at each stage. In the drug release study, we introduced a dialysis model to simulate the drug release and diffusion process in vitro. The absorbance ratio $A_{401\ nm}/A_{530\ nm}$ was proposed as an index for real-time, in situ quantification of drug release from the carrier surface, and the diffusion of the drug was simultaneously monitored by UV/Vis spectrophotometry. This strategy not only proves that AF4 can be used to effectively evaluate the drug release profile in real time, but also overcomes the inconsistency of standard evaluation methods caused by multiple separation and purification steps.

2. Materials and methods

2.1. Materials

Gold (III) chloride trihydrate ($HAuCl_4 \cdot 3H_2O$, ≥49.0 % Au basis), Sodium citrate ($C_6H_5Na_3O_7$, ≥98.0 %), Sodium phosphate dibasic dihydrate (Na_2HPO_4 * $2H_2O$, ≥99.0 %), Sodium phosphate monobasic dihydrate (NaH_2PO_4 * $2H_2O$, ≥99.0 %), Sodium chloride (NaCl, ≥99.0 %), Potassium Phosphate Monobasic (KH_2PO_4, ≥99.0 %), Bovine serum albumin (BSA, ≥98.0 %), and Dimethyl sulfoxide (DMSO, GC 99.7 %) were purchased by Sigma Aldrich (St. Louis, MO, USA). Potassium chloride (KCl, ≥99.5 %) and curcumin ($C_{21}H_{20}O_6$, ≥97.0 %, mixture of curcumin, demethoxycurcumin, and Bisdemethoxycurcumin) were obtained by Fluka. These salts were used to prepare Phosphate Buffer Saline (PBS) 1 × solution (NaCl 8 g/L, KCl 0.2 g/L, $Na_2HPO_4 \cdot 2H2O$ 1.43 g/L and KH_2PO_4 0.2 g/L), which was used as the mobile phase and diluent solution to mimic a physiological environment. All AuNPs solutions were prepared with purified 18 MΩ water. Glassware was cleaned with aqua regia and thoroughly rinsed with deionized water.

2.2. Synthesis of gold nanoparticles (AuNPs)

Citrate gold nanoparticles (Citrate-AuNPs) were synthesized using a simple wet chemical method, as described in previous literature [33]. Briefly, 100 mL of $HAuCl_4$ (1 mM) was heated to boiling, at which point 6 mL of freshly prepared sodium citrate solution (38.8 mM) was immediately added under vigorous stirring. The addition of sodium citrate, known for its reducing and stabilizing properties, initiates a series of reactions in which the color of the solution rapidly changes from pale yellow to colorless and then to dark purple. This color transition is indicative of the reduction of $HAuCl_4$ to elemental gold and the subsequent formation of AuNPs. The reaction was maintained for 15–30 min, during which time the NPs grew and stabilized, with the dark purple hue suggesting the presence of particles within a specific size range. Stirring was continued throughout the cooling process until the solution reached room temperature. The resulting AuNPs were then stored at 4 °C for further use.

2.3. Synthesis of AuNPs-BSA conjugates

In this work, we primarily focused on citrate-coated AuNPs as the main subject of investigation. In the previous chapters, we thoroughly characterized the bioconjugates formed by these nanoparticles. Compared to PEG-protected AuNPs, citrate-coated AuNPs exhibit higher binding stability and greater resistance to environmental changes when conjugated with BSA. To maximize the yield, the Au/BSA mass ratio was set at 1:1. AuNPs were first diluted to 100 ppm in deionized water. Then, 500 μL of 100 ppm BSA was added to create a 1 mL mixture, which was incubated for 1 h at room temperature (~25 °C) in a phosphate buffer (10 mM, pH 7.4 or 6). Au-BSA bioconjugate solutions of different concentrations were prepared by simultaneously varying the concentrations of the reactive monomers.

2.4. Formation of drug carriers: Au-BSA-CUR

The general method of drug deposition is as follows: DMSO was chosen as the drug solvent, and 200 μL of a curcumin solution (0.5 mg/mL) was added dropwise to the colloidal Au-BSA conjugates to achieve a final drug concentration of 0.1 mg/mL. The mixture was then incubated for 4 h in a water bath at (37 ± 1) °C with continuous stirring at 500–1000 rpm. The prepared sample was stored overnight at 4 °C to ensure complete reaction. The Au-BSA-CUR carriers and any excess curcumin were separated by centrifugation at 12,000 rpm for 7 min or by AF4. A UV-2600i SHIMADZU UV/vis spectrophotometer (Shimadzu, UK) was used to measure the absorbance spectra of all AuNPs and their derivatives.

$$LE = (\text{Total curcumin} - \text{Free curcumin}) \,/\, \text{Total curcumin} * 100\ \%$$

To determine the loading efficiency (LE), the concentration of free drug in the supernatant was measured using a UV spectrophotometer. A calibration curve for pure curcumin in DMSO was established by preparing solutions containing different concentrations of curcumin (2.5 μg/mL, 5 μg/mL, 7.5 μg/mL, 10 μg/mL, and 15 μg/mL) and measuring their absorbance at 401 nm using a UV–Vis spectrophotometer. The absorbance values were plotted against the concentrations to obtain a linear regression equation. The LE of the Au-BSA-CUR carriers was then calculated using the linear regression equation and the LE formula.

2.5. Size and morphology characterization

To ensure the accuracy of the sample size information, three primary

characterization techniques were used in this study: offline dynamic light scattering (DLS), scanning electron microscopy (SEM), and AF4 coupled online multi-angle light scattering (MALS). First, the products from each stage of the synthesis process were divided into two portions. One portion was subjected to centrifugation, while the other was purified using the AF4 platform. After purification, the samples from both methods were collected and subjected to further analysis using DLS and SEM.

A DynaPro NanoStar DLS (Wyatt Technology Corporation, USA) with a laser wavelength of 662 nm was used for hydrodynamic diameter characterization of synthesized AuNPs, Au-BSA conjugates, and Au-BSA-CUR carriers at different stages. A quartz microsample cell (JC-206) was used for all samples tested.

The FESEM (FESEM, Carl ZEISS SIGMA NTS, Germany) was operated at an accelerating voltage of 10 kV, and the samples were magnified to an appropriate level to clearly visualize the nanoparticle characteristics.

2.6. In vitro drug release experiment

Considering the inherent properties of curcumin, such as light sensitivity and susceptibility to degradation, we conducted exposure experiments on curcumin at different concentrations under controlled experimental conditions. First, fresh curcumin solutions of different concentrations (0.2 ppm, 0.5 ppm, 1 ppm, 1.5 ppm, and 2 ppm) were prepared using a solution with an optimized solvent mixing ratio (DMSO/water 1:4) as the solvent. Then, all the samples were tested by UV spectrophotometer and the corresponding spectra were recorded. The samples were then divided into two groups and subjected to light exposure and light protection for 24 h, respectively, after which the UV absorption spectra were recorded.

The drug release experiments were performed using the dialysis bag technique with a molecular weight cut-off (MWCO) 14.5 kDa containing 1 mL Au-BSA-CUR carrier solution. The MWCO was chosen to be higher than the curcumin but lower than the AuNPs and BSA to avoid the error from sample stability. First, the drug release experiments were performed in a water bath setup under different temperatures: (20 ± 1) °C (i.e., room temperature), (30 ± 1) °C, and (37 ± 1) °C. The dialysis bag was immersed in a reservoir containing 50 mL fresh PB buffer (10 mM, pH 7.4) with a shaking speed of 100 rpm. At each time point, 1 h, 2 h, 4 h, 8 h, 24 h, 30 h, 48 h, and 52 h, the samples were extracted from the reservoir for UV measurements to monitor the drug diffusion behavior. To avoid the effect of concentration changes on drug diffusion, the solution was poured back into the reservoir after each UV measurement. The diffusion percentage is calculated based on the monitored signal intensity corresponding to the standard curve at 401 nm, as shown in Fig. S6. Meanwhile, 20 μL sample from the dialysis bag was injected to the AF4 instruments to monitor the real-time drug release from the Au-BSA-CUR carrier surface. In addition, to prevent the reduction of drug carriers from affecting the total amount of drug released, a control group with the same drug carriers was established to perform release studies under identical conditions (1 mL of pure curcumin (0.1 mg/mL) contained in a dialysis bag and placed it in the reservoir). At each time point, drug carriers were extracted from the control group to supplement the missing drug carriers in the experimental group.

2.7. AF4 multidetector platform setup

An AF-2000 AF4 system (Postnova Analytics, Germany) was used for sample separation, identification, and characterization, which contains a Postnova PN7520 solvent degasser, two Postnova PN1130 Isocratic Pumps and a special cross-flow control to deliver the flow of PB buffer (10 mM, pH 7.4). The separations were performed using a 10 kDa MW cutoff regenerated cellulose membrane in a 300 mm channel with 350 μm thick spacer. The system is followed by a PN3242 4-channel UV–Vis/DAD detector and a 21-angle multiangle light scattering detector, MALS (PN3621). NovaFFF version 2.2.0.1 software was used to control the instruments, set separation parameters, collect data, handle signals from the detectors (MALS and DAD), and compute the radius and molar mass of particles during measurements.

Method optimization has extensively been described in a previous work [21]. To enhance the separation efficiency, an exponential decay model was applied to the cross-flow rate. This model gradually reduced the cross-flow from 3 mL/min to 0.4 mL/min over the course of 10 min, followed by a linear reduction to 0 mL/min over the next 15 min. Throughout the process, the detector flow was kept constant at 0.5 mL/min to maintain a stable baseline. After each injection, a 5-min rinse step was performed to ensure the complete elution of all species from the channel. Detailed operating parameters are summarized in Table S1. Four different wavelengths (280 nm, 525 nm, 435 nm, and 401 nm) were monitored to identify the species in the mixture.

3. Results and discussion

3.1. Preparation and characterization of Au-BSA-CUR carriers

The Au-BSA-CUR carriers were prepared by mixing the synthesized Au-BSA conjugates and specific concentration of curcumin solution. In previous chapters, the synthesis conditions and quantification of Au-BSA conjugates were studied and discussed in detail. For curcumin, the ratio of DMSO and water is crucial for the drug loading process due to its poor aqueous solubility. Therefore, it is very important to screen out the optimal organic/water solvent ratio, which directly influences the drug loading efficiency and the stability of the carriers. While keeping the mass ratio of drug and conjugates in the solution constant, the drug loading efficiency (LE) gradually decreases as the proportion of organic solvent gradually increases, as shown in Table 1. Considering the structure of curcumin, we also tried to improve the LE by adjusting the pH of the Au-BSA conjugate system from 7.4 to 6. This action further increased the drug LE from 68.8 % to 88.9 %, which can also be easily judged from the color of the sample supernatant after centrifugation. Therefore, the Au-BSA-CUR carriers should also have the potential for pH-controlled release. However, to ensure that the drug carrier remains stable and functional in an environment similar to body fluids, the experiments in the upcoming series were conducted under in vitro conditions with a pH of 7.4 carefully maintained throughout.

The UV/Vis technique was used to rapidly monitor the spectral changes and the rapid formation of Au-BSA-CUR carriers. As shown in Fig. 1 A, the absorbance of pure curcumin and gold nanoparticles was observed at different wavelength regions, specifically 435 nm and 528 nm. Upon the formation of Au-BSA-CUR carriers, the absorbance peaks shifted to 401 nm and 530 nm. Notably, each stage exhibited a unique UV absorbance profile, with no overlap, providing a solid basis for identification and quantification using a DAD detector during AF4 characterization. The synthesized Au-BSA-CUR carriers can be purified by centrifugation and resuspension. The mixture (AU-BSA-CUR-MIX), precipitation (AU-BSA-CUR-PRE), and supernatant (AU-BSA-CUR-SUP) were stored at 4 °C for one week to evaluate sample stability. As shown in Fig. 1, a significant signal attenuation was observed in the drug absorbance region (~400 nm) for both AU-BSA-CUR-MIX (46 %) and AU-BSA-CUR-SUP sample (53 %) after one week, while the signal of the AU-BSA-CUR-PRE sample had an attenuation ratio of 23 % at 400 nm (compared to Au-BSA conjugates) and had the same absorbance intensity at 530 nm. Therefore, we can conclude that the signal

Table 1
Sample concentration, mixing ratio (total volume 1 mL), and drug loading efficiency (LE) information.

Au-BSA (ppm)	CUR (mg/ml)	DMSO/water	LE (%)
100	0.5	1:4	68.8
107	0.4	1:3	59.7
120	0.3	1:2	49.7

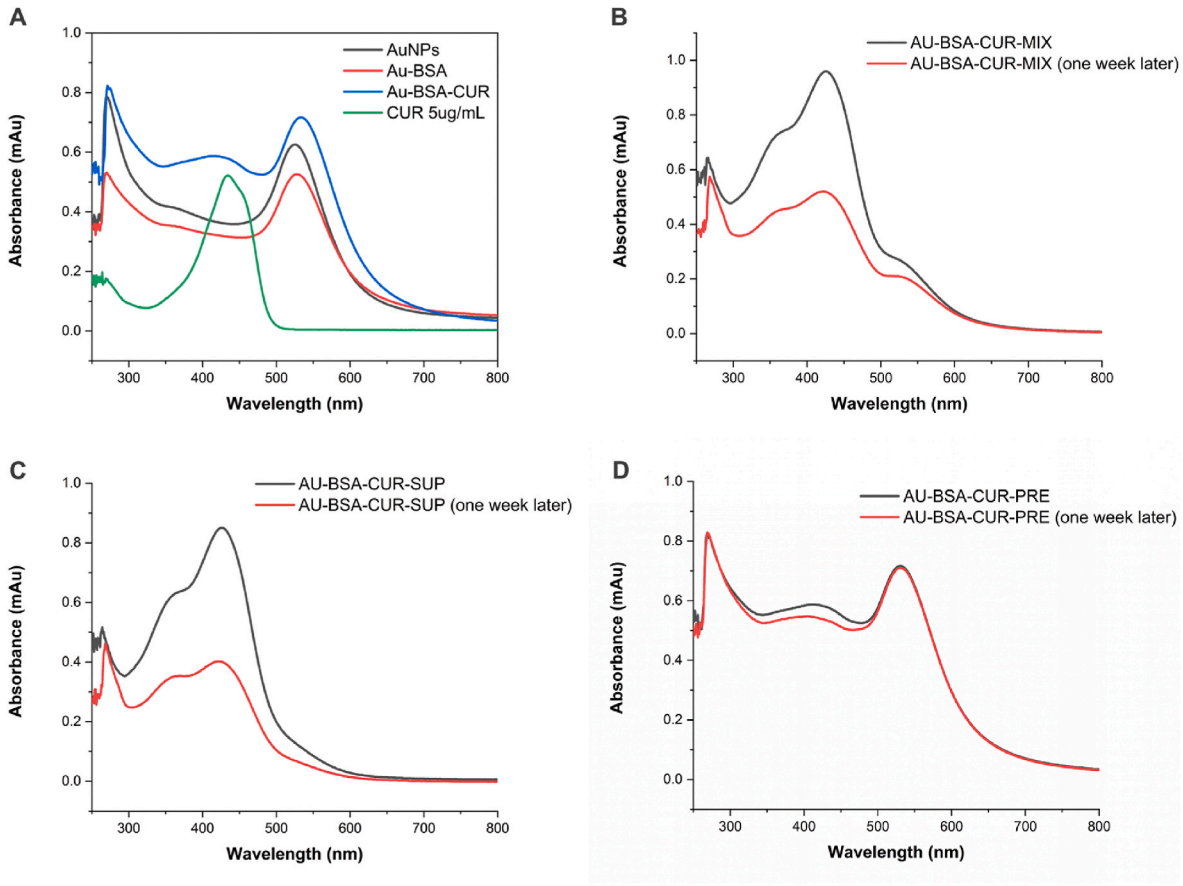

Fig. 1. The UV–Vis spectra of curcumin (5 μg/mL), AuNPs, Au-BSA conjugates, and Au-BSA-CUR carriers (A). The UV–Vis spectra of freshly prepared samples and one week later samples, (B) the mixture (AU-BSA-CUR-MIX), (C) supernatant (AU-BSA-CUR-SUP), and (D) precipitation (AU-BSA-CUR-PRE).

attenuation of the AU-BSA-CUR-MIX sample is mainly due to the degradation of free curcumin in the solution, and at the same time, the release of part of the curcumin from the Au-BSA-CUR carrier slows down the rate of drug degradation in the mixture. In addition, it is noteworthy that the AU-BSA-CUR carrier showed a remarkable ability to remain stable for a longer period after synthesis. Drug degradation did not affect the colloid properties and stability of the bioconjugates, a critical requirement for obtaining an accurate drug release profile.

Moreover, to evaluate the effect of BSA on the overall stability of drug delivery and drug loading efficiency, we performed two comparative studies (the workflow and results are shown in Fig. S2). First, one experimental group was set up by incubating the Au-BSA conjugates (purified by centrifugation) with curcumin, followed by another round of centrifugation to obtain the Au-BSA-CUR carriers and supernatant. The same experimental procedure was then performed using the Au-BSA mixture (without centrifugation) in a control experiment, which retained the excess BSA in the incubation solution. The experimental group that experienced multiple centrifugations (Au-BSA-cen-CUR-cen) has lower UV absorbance than the control group (Au-BSA-CUR-cen) at both 401 nm and 530 nm. This suggests that some of the conjugates are lost during the first centrifugation, resulting in a decrease in the total amount of conjugates. On the other hand, by comparing the absorbance intensity of the supernatants of the two samples, we can also find that the intensity of the control group (Au-BSA-CUR-cen supernatant) is significantly lower, indicating that more drug is adsorbed by Au-BSA conjugates. Indeed, the presence of excess BSA in the solution can also enhance the stability of Au-BSA conjugates, possibly due to a steric hindrance effect. In general, centrifugation not only leads to sample loss but also affects sample stability and drug uptake. Therefore, minimizing centrifugation steps during sample preparation can enhance the stability of the drug carriers and prevent a reduction in drug loading efficiency due to loss of conjugates.

3.2. Size characterization

To gain deeper insights into the effects of centrifugation at different stages of sample preparation and the stability of the synthesized bioconjugates, careful size measurements were performed at each stage using offline DLS and online MALS coupled to AF4. The samples were purified using two distinct separation methods, centrifugation and AF4, before performing DLS measurements, as shown in Table 2 (the regularization plots are shown in Fig. S3).

Notably, the hydrodynamic radius (Rh) of the samples obtained through the gentle separation method (AF4) is close to with the theoretical values, showing improved stability even one week later. Conversely, samples purified by centrifugation show an increase in Rh. Harsh purification methods not only compromise sample stability but also alter its inherent properties during the resuspension process.

Table 2
Size information from DLS and MALS. Rg from online AF4-MALS; Rh (Centrifuge) from DLS of samples purified by centrifugation; Rh (AF4) from DLS of samples collected from AF4; Rg/Rh: shape factor).

Sample name	Rg (nm)	Rh (Centrifuge, nm)	Rh (AF4, nm)	Rg/Rh
AuNPs	7.4	12.7	11.2	0.66
AuNPs-BSA	12.20	20.31	19.40	0.63
Au-BSA-CUR	13.50	21.20	19.90	0.68
Au-BSA-CUR (one week later)	13.20	27.41	18.94	0.70

Therefore, simplifying the centrifugation step in the synthesis process is considered more advantageous for subsequent applications as it preserves the natural characteristics of samples.

To further verify the accuracy of the results, we performed SEM tests on the AuNPs and AuNPs-BSA bioconjugates after centrifugation, as shown in Fig. 2. By comparing the two samples, we found that AuNPs with exposed surfaces tend to aggregate in solution, and no obvious gaps can be observed in the local magnified image (Fig. 2 A inset). In contrast, BSA-protected AuNPs exhibit relatively high monodispersity and remain more uniformly distributed even after drying, which may contribute to the steric hindrance effect of BSA. Therefore, from this perspective, BSA was successfully attached to the surface of the AuNPs, which significantly improved the stability of the sample. It is worth mentioning that the sample size obtained by SEM examination is closer to the data obtained by MALS measurement, indicating that the online coupled MALS detector can maximize the accuracy of sample size information under in situ conditions.

3.3. AF4 characterization of drug loading on the Au-BSA bioconjugates

As a soft separation method, AF4 provides a more intuitive way to monitor the samples in situ without changing their original properties. At the same time, by combining online multi-detectors, DAD and MALS, we can easily distinguish them and analyze their size distribution and shape information. The Au-BSA mixture sample and the Au-BSA-CUR mixture sample (room temperature and 37 °C) were directly injected into the AF4 system. Initially, when curcumin reacts with the Au-BSA conjugates, its maximum absorbance wavelength shifts from 435 to 401 nm. Hence, 401 nm is used as the primary monitoring wavelength to show the spectral changes before and after drug loading. Meanwhile, 280 and 530 nm serve as important internal references to track the stability of Au-BSA conjugates.

In the case of the Au-BSA mixture, based on size information, BSA was expected to be eluted first from the channel, followed by the Au-BSA conjugates. As shown in Fig. 3 A, BSA and its dimer were eluted at 7.5 min and 9 min, respectively (280 nm), while the Au-BSA conjugates were eluted at 17.5 min (280 nm and 530 nm), which demonstrates the successful synthesis of Au-BSA conjugates. For the Au-BSA-CUR mixture sample at room temperature, the chromatograms changed at both 280 nm and 401 nm, as shown in Fig. 3 D. Compared to the pre-drug loaded state, the fractogram at 401 nm revealed new peaks corresponding to the elution region of BSA (7.5 min and 9 min), implying not only the successful adsorption of curcumin on BSA but also the loading on the Au-BSA conjugates surface. However, we also observed an absorbance peak between 10 and 15 min, which never appeared before. Through three-dimensional (3D) and two-dimensional (2D) spectral analysis of both samples (Fig. 3B and C and Fig. 3 E, F), we can confirm that there is no characteristic absorbance of AuNPs and BSA in this region, but the unique spectrum of curcumin. Therefore, this peak is attributed to sample precipitation caused by the hydrophobicity of curcumin at room temperature or insufficient stirring.

Further studies were performed by placing the mixture sample in a 37 °C water bath with constant stirring. During re-injection we found that not only the drug deposition peak disappeared, but also the absorption intensity at each wavelength was improved, as shown in Fig. 3 G and 3H. To better understand the drug loading and release, we introduced for the first time the absorbance ratio ($A_{401\ nm}/A_{530\ nm}$) as an index to judge the amount of drug on the surface of conjugates. In previous work, we have repeatedly verified that the ratio ($A_{401\ nm}/A_{530\ nm}$) is a constant for Au-BSA conjugates, 0.54 ± 0.01 ($n > 3$). Under fixed conditions, the ratio can potentially reach up to 0.77 ± 0.01 ($n > 3$). Furthermore, during multiple synthesis processes, we found that even if the conjugate partially aggregates due to external conditions, the ratio remains stable until the drug release. Therefore, the comparative analysis between AF4-DAD versus traditional centrifugation followed by UV monitoring underscores the unique advantages of AF4-DAD in the context of characterizing Au-BSA-CUR carriers in the mixture, while the centrifugation-UV monitoring fails to detect a decrease in loading efficiency ($A_{401\ nm}/A_{530\ nm} = 0.64$) due to hydrophobic drug aggregation. In addition, drug aggregates cannot be filtered by the AF4 membrane, and their presence is expected to be identified during the subsequent drug release process, which is more conducive to our understanding of the behavior of hydrophobic drugs during delivery and release.

For comparison with the UV characterization data, we also performed AF4 characterization on the Au-BSA-CUR mixture sample retained for one week. As the storage time increases, the signal intensity of the sample is inevitably affected, and its retention time is also slightly shifted. Furthermore, by plotting the size as a function of distribution and cumulative, the stability and behavior of samples in the solution at different stages becomes more visible, as shown in Fig. 4. The gyration radius (Rg) of both Au-BSA conjugates and Au-BSA-CUR drug carriers are concentrated at 10–13 nm, except for the drug carriers where a small part of nanoparticles with Rg higher than 15 nm exist (≤5 %). However, when the sample was kept at room temperature for one week, their size distribution becomes broader and more than 50 % particles have Rg less than 10 nm, which means the drug carriers dissociates and aggregates significantly in solution. Notably, this critical information related to drug quantification cannot be obtained by UV characterization and offline DLS characterization. Therefore, the potential applications of the AF4 multi-detector system in the field of drug release and real-time monitoring are more prominent.

3.4. Effects of experimental conditions on curcumin

The limited bioavailability of curcumin is primarily attributed to its hydrophobic nature, which leads to instability in aqueous solutions and rapid hydrolysis with subsequent molecular fragmentation under physiological pH conditions [31]. Surprisingly, despite these challenges, the degradation products of curcumin exhibit greater aqueous solubility compared to curcumin itself, and they exhibit similar biological activities in addressing various diseases [32]. Consequently, whether the inherent low stability of curcumin is a drawback or an advantage

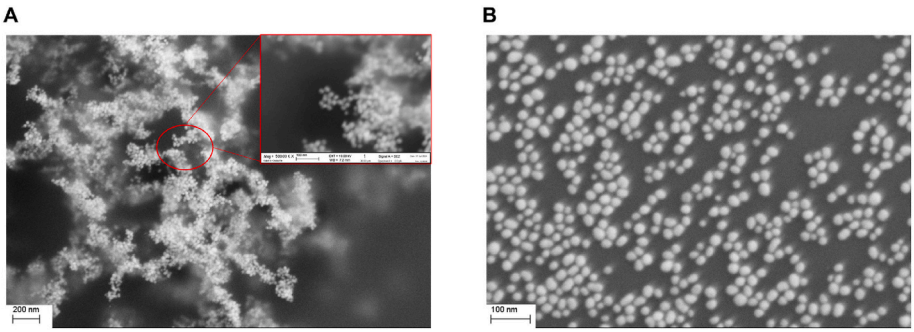

Fig. 2. The SEM imaging of (A) AuNPs (insert: local magnified image: scale bar 100 nm) and (B) Au-BSA sample after centrifugation.

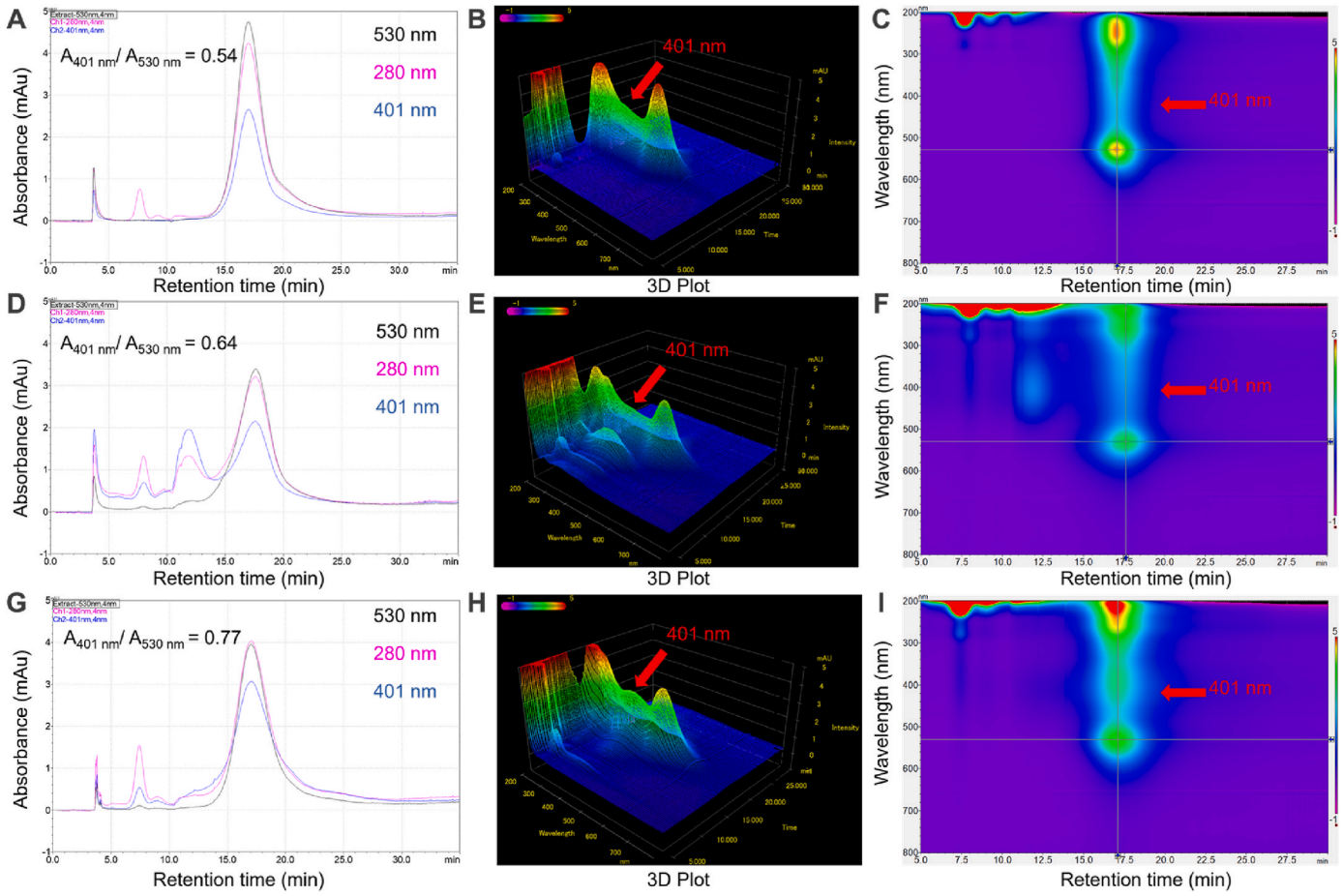

Fig. 3. AF4-DAD fractograms of Au-BSA (A), Au-BSA-CUR synthesized at room temperature (D), and Au-BSA-CUR synthesized at 37 °C (G) (curcumin 0.1 mg/mL), detection via UV 280 nm (pink), 401 nm (blue), and 530 nm (black). The representative 3D (B, E, and H) and 2D (C, F, and I) spectra were plotted. Drug loading factor: $A_{401\ nm}/A_{530\ nm}$ (maximum signal absorbance of nanocarriers at 401 nm and 530 nm). (For interpretation of the references to color in this figure legend, the reader is referred to the Web version of this article.)

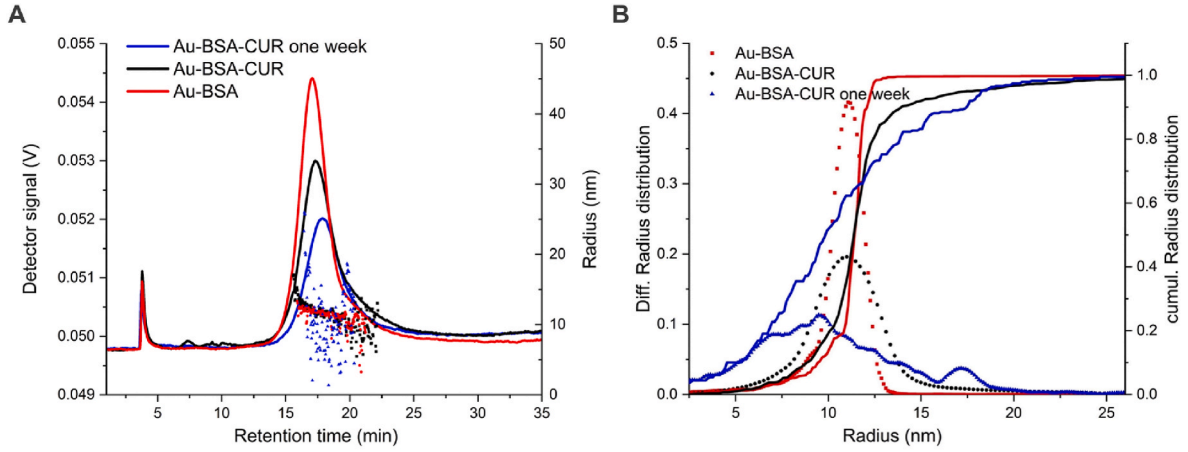

Fig. 4. Overlay of AF4-UV/Vis fractograms at 530 nm and relative size distribution (Rg) from MALS detector (A). The differential radius distribution and cumulation radius distribution (B). Au-BSA (red), Au-BSA-CUR (black), Au-BSA-CUR one week (blue). (For interpretation of the references to color in this figure legend, the reader is referred to the Web version of this article.)

remains unclear. However, the degradation will be a challenge to accurately monitor drug release profile. Therefore, it is extremely necessary to detect the UV spectral changes of curcumin in the solution under release conditions, which will help us locate the sample absorption band during the monitoring process.

Pure curcumin of different concentrations was dispersed in a DMSO/water (1:4) solvent mixture and then tested under identical conditions, with one group exposed to light for 24 h and the control group protected from light, as shown in Fig. S4. Under light-proof conditions, the UV absorbance spectrum of the sample barely changed within 24 h, while

under light-exposure conditions, the signal at 401 nm was attenuated by up to 60 %. However, it is noteworthy that the absorbance at 270 nm increases under illumination conditions. Considering the structure of curcumin, the peak at 270 nm corresponds to the absorbance band of its degradation products, Fig. 5 B [32]. Therefore, the effect of light on the drugs is significantly greater than the degradation of the drugs in aqueous solution. Under light-proof conditions, the drug can remain stable in the mixed solution for 24 h, which is crucial for using the AF4 multi-detector platform to accurately monitor the drug release curve.

In addition, to study the diffusion behavior of the drug, 1 mL of pure curcumin (0.1 mg/mL) was placed in a dialysis bag and placed it in the reservoir (10 mM PB, pH 7.4) to observe whether meaningful absorbance band would appear in the reservoir after a period of time. Unlike the conditions in the light experimental study, the reservoir used here does not contain any organic solvents. As shown in Fig. 5 A, the UV absorbance intensity at 270 nm of the sample extracted from the reservoir gradually increases over time and eventually stabilizes. Similarly, the absorbance at 401 nm follows the same increasing trend. We observed that the UV spectrum of the solution extracted from the reservoir shows absorption features of curcumin (270 nm and 401 nm), although they were not entirely consistent with the original. This suggests that the sample underwent rapid degradation after diffusion into the external reservoir, ultimately resulting in its degraded form, which is determined by the properties of curcumin.

When the impact of experimental conditions on curcumin is fully understood, it becomes easier to make accurate judgments regarding the data collected during the monitoring process. Although the samples degraded after diffusion, we can still monitor their presence by measuring the absorbance at 270 nm or 401 nm, since both wavelengths exhibit the same growth trend. The absorption at 401 nm might correspond to different intermediates or partially degraded forms of the drug compared to those at 270 nm.

3.5. In vitro drug release

In the next stage of drug release, we adopted a dialysis bag-assisted release model, as it is a standard procedure for these kind of evaluations, and it can lead to simultaneous benchmark characterization of release and evaluation of our platform performance [34–37]. In this setup, we monitored both the real-time drug release curves and the diffusion curves of the Au-BSA-CUR carriers at different temperatures. These spectral signatures provide evidence that the original drug compound undergoes chemical changes before or during the diffusion process, resulting in the presence of its degraded form in the solution, as shown in Fig. 6. The 200–300 nm region is often crowded with overlapping peaks from various substances, including solvents and other potential contaminants, suggesting that absorbance at 270 nm may not be sensitive enough to detect small differences in diffusion amounts at these temperatures. By converting the absorbance intensity at 401 nm into drug diffusion percentage, we can construct a drug diffusion profile, as shown in Fig. 6 D. As expected, higher temperatures facilitate drug diffusion, allowing diffusion equilibrium to be reached within 10 h, while at lower temperatures, equilibrium may be delayed to 24 h or longer.

To further ensure the accuracy of the experiment, we also monitored the trend of the absorbance intensity at 270 nm over time at different temperatures, as shown in Fig. S5. The changes in absorbance intensity at 270 nm showed a similar trend to that at 401 nm. However, the observation that the total amount of drug diffusion at different temperatures (20 °C and 30 °C) shows minimal variation using 270 nm absorbance suggests that temperature may not be the only factor within this range. In other words, this temperature-dependent drug diffusion is understandable; however, the existing data do not allow us to determine whether the degradation rate of the drug also influences the diffusion process. These data not only suggest the presence of a potentially stable and robust release mechanism from drug carrier solutions but also underscore the need to explore additional conditions or employ alternative monitoring methods to fully understand the diffusion process.

3.6. AF4 multi-detector platform for drug release profile

The observation that the total amount of drug diffusion at different temperatures (20 °C and 30 °C) shows minimal variation using 270 nm absorbance suggests that temperature may not be the only factor within this range. This indicates a potentially stable and robust release mechanism but also highlights the need to explore other conditions or monitoring methods to gain a more complete understanding of the diffusion process. Therefore, we simultaneously monitored the sample release behavior from the surface of Au-BSA-CUR carriers by extracting samples from the dialysis bag at the same time points and injecting them into the AF4 multi-detector system. AF4 allows for real-time monitoring of the release process, providing immediate insight into the kinetics of drug release from the Au-BSA-CUR carrier. This dynamic analysis can not only help establish a real-time drug release curve but also simultaneously track the behavior of the released drug in the solution, providing a more comprehensive understanding of the drug diffusion data.

Real-time assisted monitoring using the AF4 multi-detector platform allows us to gain a multifaceted understanding of the behavior of drug carriers under release conditions, as shown in Fig. 7. The wavelengths of 530 nm (Fig. 7A–C, and E) and 401 nm (Fig. 7B–D, and F) were used to monitor the stability of drug carriers and to investigate possible drug aggregation phenomena, respectively. As presented in Fig. 7A–C, and E,

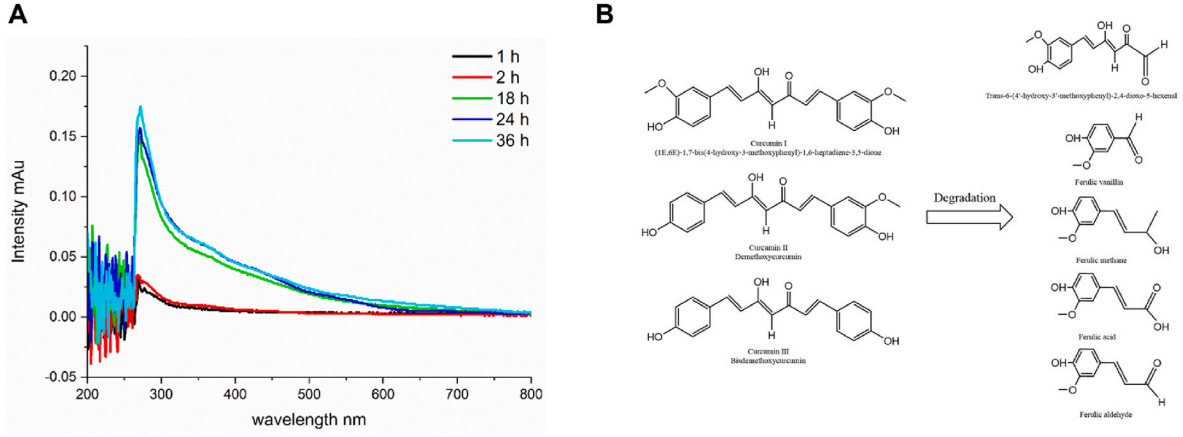

Fig. 5. (A) The UV spectra of samples extracted from the reservoir (10 mM PB, pH 7.4) at different time points. (B) The main structural forms of curcumin and its degradation products (drawn using Chemdraw 19.0).

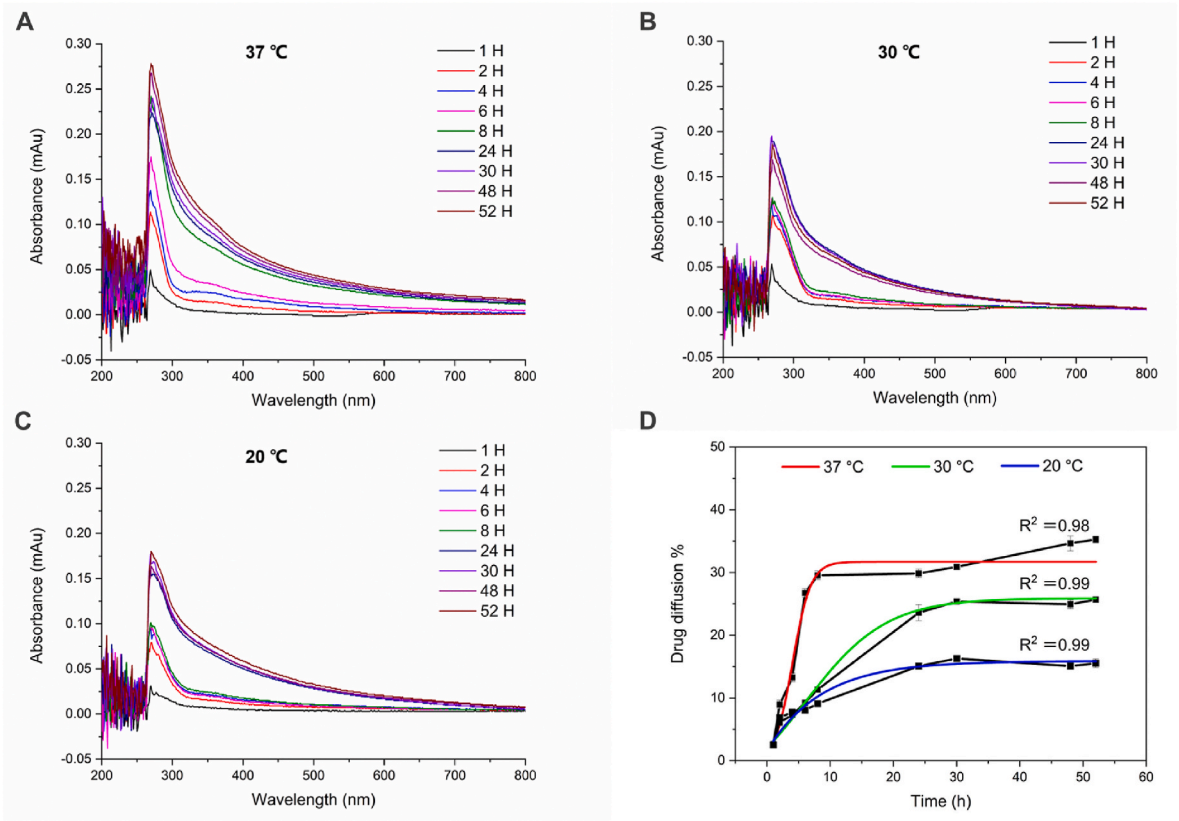

Fig. 6. The UV spectra of samples extracted from the reservoir (10 mM PB, pH 7.4) at different time points and different temperatures (A) 37 °C, (B) 30 °C, and (C) 20 °C. (D) Drug diffusion profile under different temperature conditions (The diffusion percentage is calculated based on the monitored signal intensity corresponding to the standard curve at 401 nm, shown in SI).

the stability in size distribution and retention time indicates that the carrier maintains its structural integrity and does not degrade or change its properties over the range of temperatures studied, which is crucial to ensure consistent drug release profiles. In addition, a stable size distribution ensures that each carrier particle behaves similarly, resulting in uniform release rates and better predictability in drug delivery. It is worth noting that at 20 °C, the signal at 530 nm decayed after 48 h (Fig. 7 E), but no impurities or meaningful signal peaks appeared in the chromatography, indicating that the sample was partially aggregated in the dialysis bag, which can also visible in the dialysis bag. The reliable performance and size distribution observed before 48 h provide valuable data on the initial drug release. In contrast, at 37 °C, the signal at 530 nm did not decay, but impurity peaks appeared at 48 and 52 h. These impurity peaks were not present before this time and were also observed in the 401 nm chromatogram. Therefore, we attributed them to system-induced impurity peaks or partial sample carryover caused by multiple injections, but it did not affect the experiment.

The distinct differences in chromatogram behavior at 401 nm at different temperatures highlight the importance of temperature in influencing drug release and degradation processes, as shown in Fig. 7B–D, and F. It is particularly noteworthy that new peaks appeared in the 10–15 min range below 30 °C, and 20 °C (red dotted box in Fig. 7 D and F). These peaks correspond to the locations where drug aggregates were observed, as discussed in the previous section. In the discussion, we noted that this peak can be avoided during the synthesis process by ensuring sufficient stirring and maintaining a 37 °C water bath, which can help to prevent aggregation and thereby improve drug loading efficiency. However, the results of the actual monitoring process indicated that, despite using a water bath at the appropriate temperature and ensuring sufficient stirring, the aggregation peaks persisted in these samples. We believe that drugs released from the surface partially aggregate at lower temperatures due to hydrophobic effects and gradually degrade over time, while at higher temperatures, the aggregation is not obvious and is replaced by rapid degradation. Based on these analyses, the slower diffusion and longer time to reach diffusion equilibrium at lower temperatures can be attributed to both thermodynamic factors and the aggregation of curcumin.

The main peak signals showing a decreasing trend indicate that there is a reduction in the concentration of the primary drug component on the surface of Au-BSA-CUR carriers. By taking the ratio of absorbance at 401 nm–530 nm ($A_{401\ nm}/A_{530\ nm}$), variations due to baseline drift or overall signal intensity changes can be normalized, making it easier to detect relative changes in the drug concentration, as shown in Fig. 8. Comparing drug diffusion, the drug release phase can be completed within 10 h, regardless of the temperature, while the total amount of drug released and the rate of release differ significantly between lower and higher temperatures. Therefore, rapid drug release of the at low temperatures, coupled with slower diffusion into the external solution, leads to partial aggregation due to hydrophobic interactions. This understanding highlights the importance of considering both the release kinetics and diffusion dynamics in the formulation and storage of drug delivery systems. Of particular note is that the drug is not fully released under any temperature conditions. During subsequent long-term monitoring, the release factor ($A_{401\ nm}/A_{530\ nm}$) tends to stabilize, indicating that the drug has not undergone further degradation on the carrier surface. This conclusion is supported by UV spectrum analysis at the corresponding time points, where the peak at 270 nm remains stable (Fig. 6). With a ratio of 0.77 as full load, the maximum drug release that can be achieved at 37 °C is 34.8 %.

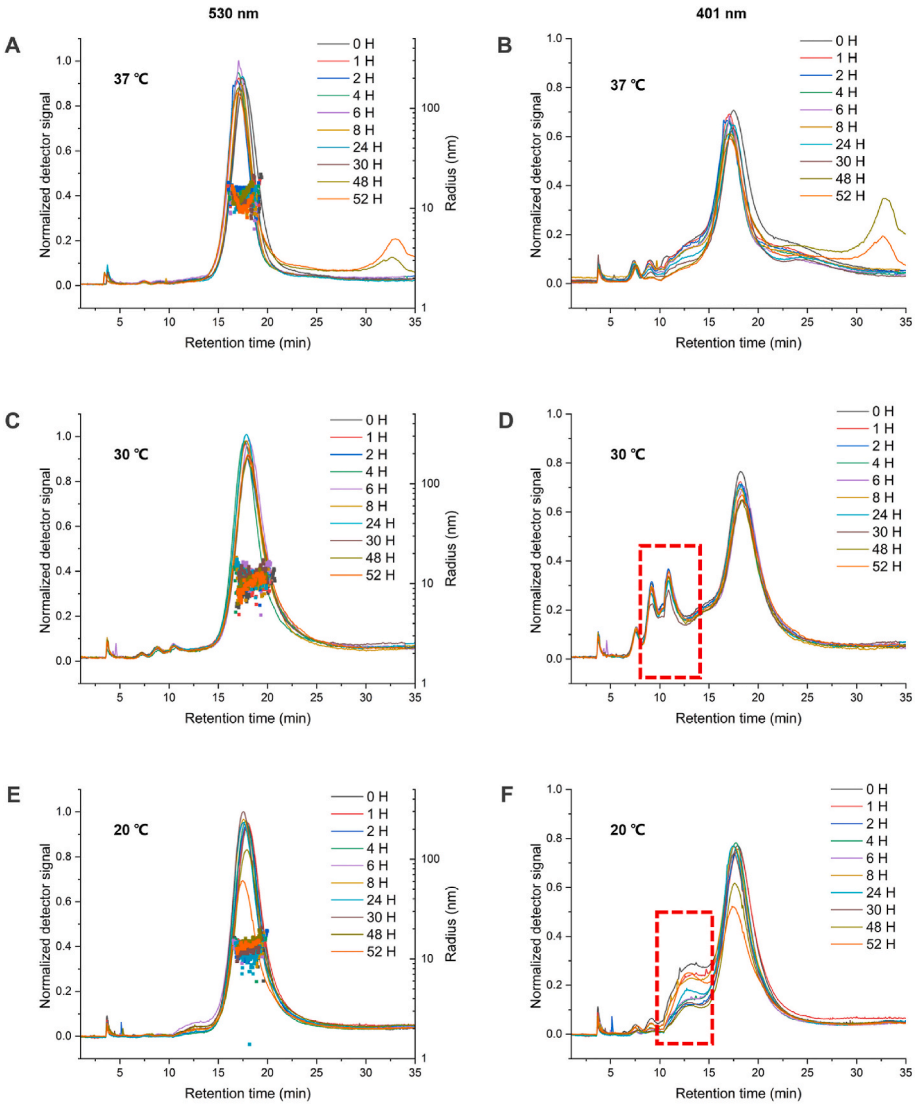

Fig. 7. Normalized AF4-$UV_{530\ nm}$ (A, C, and E (left axis)) and AF4-$UV_{401\ nm}$ (B, D, and F) fractograms of Au-BSA-CUR carriers and their relative size distribution (Rg, A, C, and E (right axis)) at different time points under 37 °C, 30 °C, and 20 °C conditions. Rg is gyration radius from MALS detector. The red dotted box represents highlighting. The fractograms and corresponding Rg data are color matched. (For interpretation of the references to color in this figure legend, the reader is referred to the Web version of this article.)

4. Conclusion

In summary, we have successfully developed a competitive strategy for real-time in-situ characterization of the drug release profile based on the AF4 multi-detection system. By combining detailed offline characterizations (such as DLS and UV–Vis spectroscopy) with advanced online characterizations (such as DAD and MALS), this study successfully optimized the drug carrier synthesis and characterization process and established a unified evaluation standard for subsequent drug release profile monitoring. Firstly, the combination of online MALS and offline DLS measurements highlighted the effect of centrifugation on the size distribution and stability of drug delivery systems. The real-time size-resolved sample information provided by AF4 helped to identify the subtle differences in the drug delivery system's resistance to different conditions during the monitoring process. In addition, the comparative analysis between AF4-DAD and traditional centrifugation followed by UV monitoring underscores the unique advantages of AF4-DAD in the context of characterizing Au-BSA-CUR carriers in the mixture, while the centrifugation-UV monitoring fails to detect a decrease in loading efficiency due to hydrophobic drug aggregation. These advantages make AF4-DAD-MALS a more reliable and insightful technique for studying the stability, loading efficiency, and release dynamics of nanoparticle-based drug delivery systems. Therefore, in the second phase, the real-time drug release profile was successfully constructed by plotting the ratio $A_{401\ nm}/A_{530\ nm}$ versus time. The results highlight the rapid release of hydrophobic drugs at different temperatures (within 10 h) and the inevitable aggregation behavior at low temperatures (30 °C and 20 °C), which will directly affect the further diffusion and degradation of the drugs. Furthermore, the establishment of drug diffusion curves also confirms the unreliability and unpredictable errors of real-time monitoring of easily degradable drugs using UV monitoring techniques. Overall, this work demonstrates the ability of the AF4 multi-detector technique to provide detailed, real-time and in-situ analysis, making it a powerful tool for the development and optimization of drug delivery systems. In the future, the tailoring of the release media of the most promising bioconjugates, with an "in silico" perspective, could also support release studies in simulated body fluids.

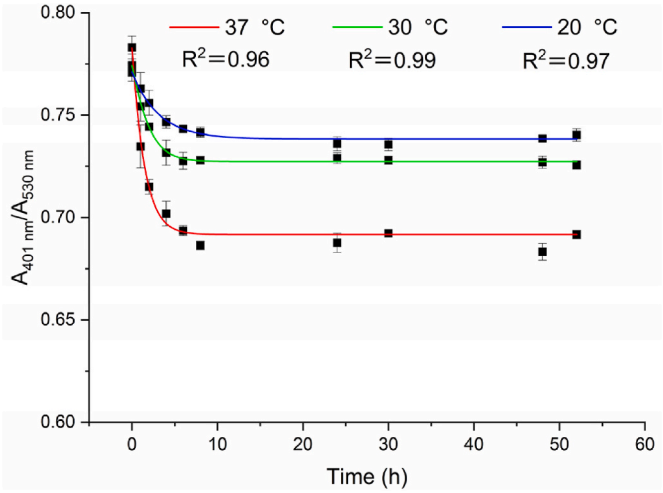

Fig. 8. Drug release profile of Au-BSA-CUR carriers under different temperature. The factor $A_{401\ nm}/A_{530\ nm}$ (maximum signal absorbance of nanocarriers at 401 nm and 530 nm).

CRediT authorship contribution statement

Valentina Marassi: Writing – review & editing, Validation, Supervision, Formal analysis, Conceptualization. **Junjie Wang:** Writing – original draft, Methodology, Investigation, Data curation, Conceptualization. **Stefano Giordani:** Writing – review & editing, Investigation, Formal analysis, Data curation. **Anna Placci:** Writing – review & editing, Investigation, Formal analysis, Data curation, Conceptualization. **Barbara Roda:** Writing – review & editing, Supervision, Resources, Funding acquisition, Conceptualization. **Pierluigi Reschiglian:** Writing – review & editing, Supervision, Resources, Project administration, Methodology, Funding acquisition, Conceptualization. **Andrea Zattoni:** Writing – review & editing, Validation, Supervision, Resources, Project administration, Methodology, Funding acquisition, Data curation, Conceptualization.

Funding

Junjie Wang's PhD grant was funded by the China Scholarship Council (CSC).

Declaration of competing interest

The authors declare that they have no known competing financial interests or personal relationships that could have appeared to influence the work reported in this paper.

Acknowledgements

We acknowledge Simona Ortelli for her support in performing SEM measurements.

Appendix A. Supplementary data

Supplementary data to this article can be found online at https://doi.org/10.1016/j.aca.2025.344246.

Data availability

Data will be made available on request.

References

[1] A.O. Oladipo, S.L. Lebelo, T.A.M. Msagati, Nanocarrier design–function relationship: the prodigious role of properties in regulating biocompatibility for drug delivery applications, Chem. Biol. Interact. 377 (2023) 110466.
[2] S. Nagpal, et al., Revisiting nanomedicine design strategies for follow-on products: a model-informed approach to optimize performance, J. Contr. Release 376 (2024) 1251–1270.
[3] M.-C. Daniel, D. Astruc, Gold nanoparticles: Assembly, supramolecular chemistry, quantum-size-related properties, and applications toward biology, catalysis, and nanotechnology, Chem. Rev. 104 (1) (2004) 293–346.
[4] L. Dykman, N. Khlebtsov, Gold nanoparticles in biomedical applications: recent advances and perspectives, Chem. Soc. Rev. 41 (6) (2012) 2256–2282.
[5] I. Zare, et al., Gold nanostructures: synthesis, properties, and neurological applications, Chem. Soc. Rev. 51 (7) (2022) 2601–2680.
[6] A. Graczyk, et al., Gold nanoparticles in conjunction with nucleic acids as a modern molecular system for cellular delivery, Molecules 25 (2020), https://doi.org/10.3390/molecules25010204.
[7] J.W. Lee, S.-R. Choi, J.H. Heo, Simultaneous stabilization and functionalization of gold nanoparticles via biomolecule conjugation: progress and perspectives, ACS Appl. Mater. Interfaces 13 (36) (2021) 42311–42328.
[8] K.C.R. Bahadur, B. Thapa, N. Bhattarai, Gold nanoparticle-based gene delivery: promises and challenges 3 (3) (2014) 269–280.
[9] S. Rastogi, et al., Gold nanoparticle-based sensors in food safety applications, Food Anal. Methods 15 (2) (2022) 468–484.
[10] R. Khandelia, et al., Gold nanocluster embedded albumin nanoparticles for two-photon imaging of cancer cells accompanying drug delivery, Small 11 (33) (2015) 4075–4081.
[11] J. Mariam, S. Sivakami, P.M. Dongre, Albumin corona on nanoparticles – a strategic approach in drug delivery, Drug Deliv. 23 (8) (2016) 2668–2676.
[12] L. Rastogi, A.J. Kora, A. J, Highly stable, protein capped gold nanoparticles as effective drug delivery vehicles for amino-glycosidic antibiotics, Mater. Sci. Eng. C 32 (6) (2012) 1571–1577.
[13] S. Lee, et al., Spatiotemporally controlled drug delivery via photothermally driven conformational change of self-integrated plasmonic hybrid nanogels, J. Nanobiotechnol. 21 (1) (2023) 191.
[14] H. Zhang, et al., Multiple-mRNA-controlled and heat-driven drug release from gold nanocages in targeted chemo-photothermal therapy for tumors, Chem. Sci. 12 (37) (2021) 12429–12436.
[15] L. Liu, et al., Controlled bio-orthogonal catalysis using nanozyme–protein complexes via modulation of electrostatic interactions, Materials 17 (7) (2024) 1507.
[16] Z. Xu, et al., Protein-nanoparticle co-assembly supraparticles for drug delivery: ultrahigh drug loading and colloidal stability, and instant and complete lysosomal drug release, Int. J. Pharm. 658 (2024) 124231.
[17] D. Bobo, et al., Nanoparticle-based medicines: a review of FDA-approved materials and clinical trials to date, Pharm. Res. 33 (10) (2016) 2373–2387.
[18] A.C. Anselmo, S. Mitragotri, Nanoparticles in the clinic, Bioeng. Trans. Med. 1 (1) (2016) 10–29.
[19] A. Zattoni, et al., Flow field-flow fractionation for the analysis of nanoparticles used in drug delivery, J. Pharmaceut. Biomed. Anal. 87 (2014) 53–61.
[20] J. Arenas-Alatorre, et al., Advantages and limitations of OM, SEM, TEM and AFM in the study of ancient decorated pottery, Appl. Phys. A 98 (3) (2010) 617–624.
[21] J. Wang, et al., Quality control and purification of ready-to-use conjugated gold nanoparticles to ensure effectiveness in biosensing, Frontiers. Sensors 3 (2022).
[22] K. Saha, et al., Gold nanoparticles in chemical and biological sensing, Chem. Rev. 112 (5) (2012) 2739–2779.
[23] J.M.V. Makabenta, et al., Nanomaterial-based therapeutics for antibiotic-resistant bacterial infections, Nat. Rev. Microbiol. 19 (1) (2021) 23–36.
[24] V. Marassi, et al., Comprehensive characterization of gold nanoparticles and their protein conjugates used as a label by hollow fiber flow field flow fractionation with photodiode array and fluorescence detectors and multiangle light scattering, J. Chromatogr. A 1636 (2021) 461739.
[25] V. Marassi, et al., Synthesis monitoring, characterization and cleanup of Ag-Polydopamine nanoparticles used as antibacterial agents with field-flow fractionation, Antibiotics 11 (3) (2022).
[26] V. Marassi, et al., FFF-based high-throughput sequence shortlisting to support the development of aptamer-based analytical strategies, Anal. Bioanal. Chem. 414 (18) (2022) 5519–5527.
[27] S. Giordani, et al., Rapid and green discrimination of bovine milk according to fat content, thermal treatment, brand and manufacturer via colloidal fingerprinting, Food Chem. 440 (2024) 138206.
[28] S. Shakiba, et al., Asymmetric flow field-flow fractionation (AF4) with fluorescence and multi-detector analysis for direct, real-time, size-resolved measurements of drug release from polymeric nanoparticles, J. Contr. Release 338 (2021) 410–421.
[29] L. Gómez-Lázaro, et al., Assessment of in vitro release testing methods for colloidal drug carriers: the lack of standardized protocols, Pharmaceutics 16 (2024), https://doi.org/10.3390/pharmaceutics16010103.
[30] S. Giordani, et al., Liposomes characterization for market approval as pharmaceutical products: analytical methods, guidelines and standardized protocols, J. Pharmaceut. Biomed. Anal. (2023) 236.
[31] S.S. Bansal, et al., Advanced drug delivery systems of curcumin for cancer chemoprevention, Cancer Prev. Res. 4 (8) (2011) 1158–1171.
[32] L. Shen, H.-F. Ji, The pharmacology of curcumin: is it the degradation products? qq 18 (3) (2012) 138–144.

[33] K. Yang, Y. Hu, N. Dong, A novel biosensor based on competitive SERS immunoassay and magnetic separation for accurate and sensitive detection of chloramphenicol, Biosens. Bioelectron. 80 (2016) 373–377.
[34] R. Schwarzl, et al., General method for the quantification of drug loading and release kinetics of nanocarriers, Eur. J. Pharm. Biopharm. 116 (2017) 131–137.
[35] Y. Yao, X. Gao, Z. Zhou, The application of drug loading and drug release characteristics of two-dimensional nanocarriers for targeted treatment of leukemia, Frontiers. Mater. 10 (2023) 1209186.
[36] G.D. Chakrapani, et al., Curcumin-loaded hybrid particles for drug delivery applications, Cleaner Chem. Eng. 4 (2022) 100066.
[37] J. Chen, et al., Fabrication and evaluation of curcumin-loaded nanoparticles based on solid lipid as a new type of colloidal drug delivery system, Indian J. Pharmaceut. Sci. 75 (2) (2013) 178.